SOVIET PHYSICS

JETP

*A translation of the Zhurnal Éksperimental'noĭ i Teoreticheskoĭ Fiziki*



Vol. 22, No. 5, pp. 949-1147 (Russ. Orig. Vol. 49, No. 5, pp. 1377-1680) May, 1966

# *DISCRETE STATES OF A PLASMA BEAM AND THE TRANSITIONS BETWEEN THEM*

M. V. NEZLIN and A. M. SOLNTSEV

Submitted to JETP editor April 8, 1965; resubmitted July 21, 1965

J. Exptl. Theoret. Phys. (U.S.S.R.) **49**, 1377-1388 (November, 1965)

It is well known [1-4] that when the component density ratio of a two-component beam consisting of a "cold" plasma column and of a fast electron flux penetrating into the column decreases, the beam goes over from a macroscopic stable state to a state with a virtual cathode. The nature of this transition is studied experimentally. It is shown that it is the result of two jumps during which the plasma-particle energy, the oscillation frequencies, radial dimensions of the beam, and its potential increase considerably. These manifestations of beam instability remain the same even if the fast-electron velocity distribution has no order whatever.

## INTRODUCTION

IT was shown earlier [1-4] that a plasma beam, that is, a column of cold plasma broached by a flux of accelerated (primary) electrons, exhibits a unique instability under certain conditions. This instability does not arise in the case when the following condition is satisfied

$$n_1 v_1 < n_2 v_2 / 4 \quad \text{or} \quad \alpha > \alpha_c, \tag{1}$$

where

$$\alpha = n_2 / n_1, \qquad \alpha_c = 4 v_1 / v_2,$$

and $n_1$, $v_1$, $n_2$, and $v_2$ are the density and average velocity of the primary (fast) and secondary (cold) electrons. If, to the contrary,

$$n_1 v_1 \gg n_2 v_2 / 4, \quad \text{or} \quad \alpha \ll \alpha_c, \tag{2}$$

then the beam instability produces inside the beam strong electric fields that cause effective heating of the plasma ions [3] and deep modulation of the electron beam ("virtual cathode" [4]).

Thus, the properties of a plasma beam were investigated only in two limiting cases: $\alpha > \alpha_c$ and $\alpha \ll \alpha_c$, and the question of the state of the beam remains open. An investigation of this question was one of the purposes of the experiments described below. Another purpose was to study the frequency spectrum of the oscillations produced in the beam in all its states, and the dependence of this spectrum on the form of the beam-electron velocity distribution function.

## 1. EXPERIMENTAL PROCEDURE

All the experiments were carried out with the installation shown schematically in Fig. 1. The plasma source employed in this installation was that described in [2]; this source operated in a continuous mode, usually at a discharge voltage $V_{dis}$ = 200—300 V and a discharge current $I_{dis}$ = (0.5—1.5) A. The source had a cathode 1 cm in diameter and a discharge chamber 2 cm in diameter and 15 cm long. The parameter $\alpha$ was varied by changing the flow of gas fed to the plasma source (in the cathode region). The working gases were argon and hydrogen. The beam receiver (anode) had a small center hole, back of which a collector

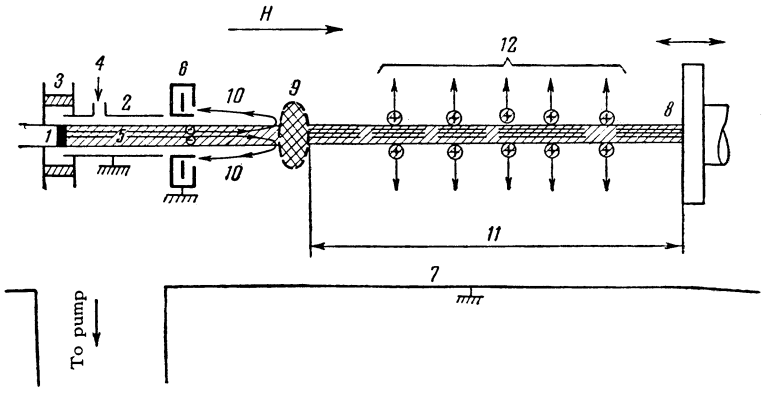


FIG. 1. Experimental setup. 1 – indirectly heated cathode of 1 cm diameter, having a negative potential – $V_{dis}$; 2 – discharge chamber, 2 cm in diameter and 15 cm long, having zero potential, with gas pressure in the chamber $p \approx 10^{-3}$ mm Hg; 3 – insulator; 4 – gas inlet; 5 – beam; 6 – ring; 7 – vacuum chamber, 30 cm diameter, gas pressure in chamber $p \approx 10^{-5}$ mm Hg; 8 – anode, 15 cm diameters; 9 – virtual cathode (negative-potential region); 10 – trajectories of electron beam at the instant of formation of the virtual cathode; 11 – positive-potential region; 12 – accelerated ions.

was placed to measure the densities of the fast electrons and the ions [1,2]. In one series of measurements, the anode could be displaced along the beam, and then the influence of the length of the beam on its state was investigated; in a second series of measurements, the anode was placed transverse to the beam, and then the radial distribution of the electrons and ions was measured. In the latter case the length of the beam was fixed at 150 cm.

Two beam modes were used: the "direct arc" mode and the "reflecting arc" mode. In the first of these modes the anode had the same potential as the discharge chamber of the plasma source and the walls of the vacuum chamber, i.e., ground potential. In the second mode the anode had the same potential as the cathode and served as a reflector of the beam electrons (Fig. 1). These modes differed in the beam-electron velocity distribution function. The "direct-arc" mode corresponds approximately to a function $f_1(v)$ [4]:

$$f_1(v) \approx \begin{cases} \text{const} & \text{when } 0 < v \lesssim +v_m, \\ 0 & \text{outside this interval} \end{cases}$$

and the 'reflected arc' corresponds to a function $f_2(v)$:

$$f_2(v) \approx \begin{cases} \text{const} & \text{when } -v_m \lesssim v \lesssim +v_m, \\ 0 & \text{when } |v| > |v_m|, \end{cases}$$

where $mv_m^2/2 = W_1 = eV_{dis}$, and $W_1$ is the energy to which the primary beam electrons are accelerated in the near-cathode layer (actually in such discharges there is always a fraction of "anomalous" electrons with $v > |v_m|$). Both distribution functions are shown schematically in Fig. 2. Unless otherwise stipulated, we refer throughout to the 'direct arc'.

The procedure for measuring the ion energies and the beam potential was the same as before [2,3].

The virtual cathode was detected by measuring the energies of the electrons moving opposite the beam, with the aid of an annular electrode 6, screened on all sides except for a narrow annular slot 21 mm in diameter and 0.5 mm wide (Fig. 1) facing the anode. If condition (2) is satisfied, the floating potential $\varphi_r$ of this ring becomes strongly negative and reaches a value equal to the potential of the cathode: $\varphi_r = V_{dis}$, thus offering evidence of formation of a virtual cathode (to this end, however, it is necessary that the length of the beam $L_b$ exceed a certain "critical length" $L_c$ of the order of 25—30 cm). The fast electrons reflected from the virtual cathode had in this case the same energy spectrum as the primary electrons moving along the beam—from the cathode to the anode; this spectrum is well described, in first approximation, by the function $f_1(v)$ of Fig. 2.

To measure the frequency spectrum of the oscillations we used in addition to the already mentioned ring also three Langmuir probes 3 mm long and 0.3 mm in diameter. One of them (No. 1) could be moved radially in the central plane of the installation, and the other two (Nos. 2 and No. 3) were secured to a stationary anode at a distance 1 cm from the axis of the beam and 60 cm from the first probe. Probes 1 and 2 were located in this case at the same azimuth, while probe 3 could be moved in azimuth through an arbitrary angle. The oscillation spectra were recorded with a panoramic spectrum analyzer (S4-8).

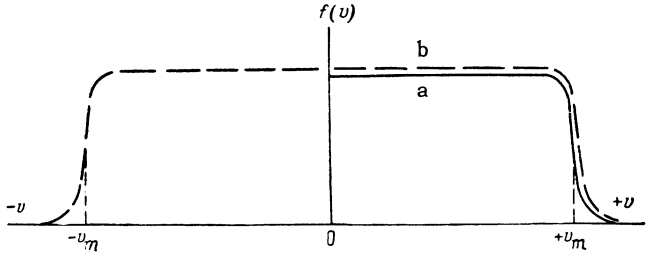


FIG. 2. Distribution function of primary electrons of the beam by velocities in two modes: a – "direct arc" $f(v) = f_1$; b – "reflecting arc" $f(v) = f_2$.

The intensity of the magnetic field could be adjusted from 1000 to 5000 Oe; in most experiments it amounted to 1400 Oe.

## 2. EXPERIMENTAL DATA

In our experiments, the state of the plasma beam was characterized by features such as the energy and the spatial distribution of the particles, the beam potential, and the frequency spectrum of the oscillations. Experiments with argon and hydrogen gave similar results. Unless otherwise stipulated, we refer in what follows to argon.

Figure 3 shows the influence of the argon flow Q into the plasma source on the total strength of the anode electron current $I_a$, on the electron current density $J_e$, and on the ion current density $J_+$ of the plasma beam axis, on the floating potential $\varphi_r$ of the annular electrode, on the beam potential $\varphi_b$ in the central plane of the installation (i.e., where it is always positive, Fig. 1), and on the first harmonic $f_0$ of the line section of the oscillation spectrum. We see that as Q is gradually varied two jump-like transitions occur in the plasma beam between three discrete states: I—$Q \gg Q_2$, II—$Q_1 < Q < Q_2$, and III—$Q < Q_1$. The essential differences between these states, in addition to those obvious directly from Fig. 3, can be traced also by examining the following indicators.

1. Energies of the electrons moving against the beam. These energies can be readily estimated from the deceleration characteristics of the ring electrode, shown in Fig. 4. We see that when $W_1 = V_{dis} = 200$ eV and the average energy of the primary electrons moving along the beam is $\sim W_1/2 \approx 100$ eV, the average energy of the electron moving opposite the beam is 2—3 eV in state I, approximately 10 eV in state II, and 100 eV in state III; in the latter case a virtual cathode is produced in the beam (at ~10 cm from the plasma source).

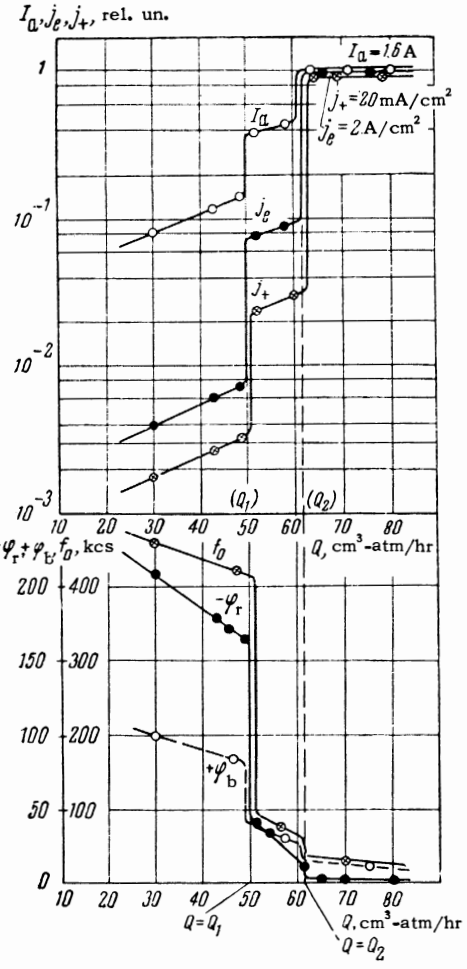


FIG. 3. Plots of $I_a$, $j_e$, $j_+$, $\varphi_r$, $\varphi_b$, and $f_0$ against the flow of argon Q in the plasma source. $V_{dis}$ = 200 V, $I_{dis}$ = 1 A, H = 1400 Oe, $p = 1 \times 10^{-5}$ mm Hg, $L_b$ = 150 cm ($\varphi_r$ and $\varphi_b$ are in volts).

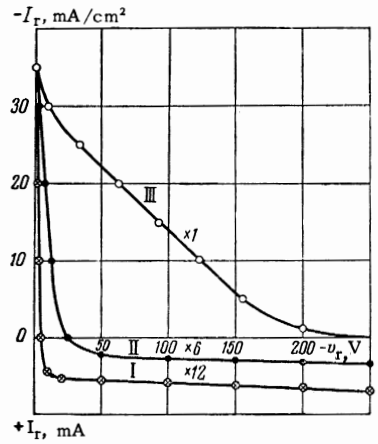


FIG. 4. Voltage-current characteristics of the annular electrode in three states of the beam. The character of the state is indicated by the corresponding Roman numeral on the curve. The conditions are the same as Fig. 3.

2. Radial distribution of charged particles. As shown in Fig. 5, in state I the radial distribution of the fast electrons coincides with the distribution of the ions and corresponds well to the diameter of the cathode. On going over to the state II, the primary beam spreads out, and the cold plasma spreads out even more strongly, so that the radial distribution of the fast electrons no longer coincides with the ion distribution. In state III further dissolution of the beam and of the plasma is observed. In accordance with the changes of the transverse dimensions of the beam and the plasma, a change takes place in the parameter $\alpha$, which is $\approx$20—30 in state I and approaches unity in state II;

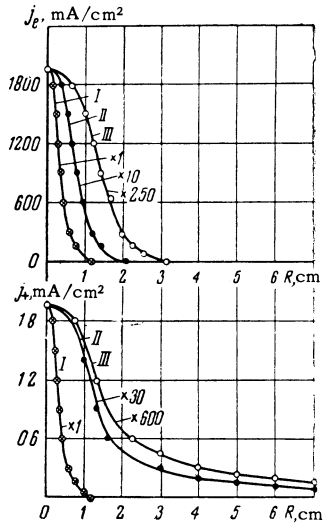


FIG. 5. Radial distribution of the ion current density $j_+$ and the primary-electron density $j_e$ in three states of the beam. The character of the state is indicated by the Roman numerals on the curves. The conditions are same as in Fig. 3.

any attempt to reduce $\alpha$ further blocks off the primary beam.

3. Ion energy $W_\perp$. In state I we have $W_\perp \approx 10-20$ eV, in state II $W_\perp$ reaches the value $W_1 = eV_{dis}$, while in state III $W_\perp$ is even larger.

4. Beam and plasma potential $\varphi_b$. It is seen from Fig. 3 that during the course of the transitions I → II → III the value of $\varphi_b$ increases from 10—15 V to 80—100 V. It must be noted here that when we speak of the beam potential we have in mind the greater part of its length—to the right of the virtual cathode, where the potential is positive in all three states of the beam (Fig. 1). In a small region of the beam the potential can assume in this case a negative value (virtual cathode in state III, Fig. 1).

5. Character of passage of the primary beam through the plasma column. In state I all the primary electrons emitted from the plasma source reach the anode, and the total electron current to the anode $I_a$ exceeds the primary-electron current $I_{dis}$ by an amount equal to the plasma-electron current. In state II all the fast electrons apparently still reach the anode, and the fact that $I_a < I_{dis}$ can be attributed to the fraction of the primary electrons that are knocked out by the beam from the anode without returning. In state III approximately 10 per cent (averaged over the time) of the primary electrons emitted from the plasma source reach the anode, while the remainder, oscillating between the cathode of the source and the virtual cathode, drift in a radial direction and are lost on the walls of the source discharge chamber.

6. Oscillation spectrum. Figure 6 shows the oscillation spectra of the current in probe No. 1 in the three states of the beam (the potential of the

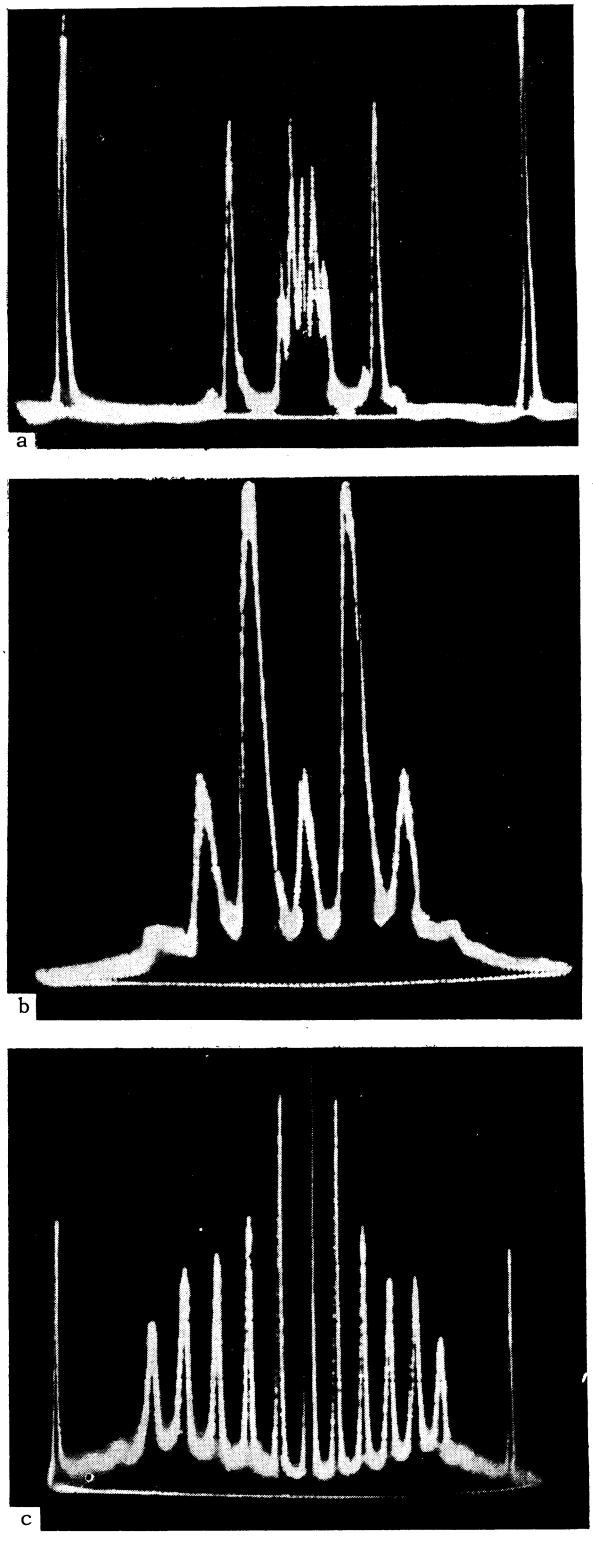


FIG. 6. Spectra of oscillation of the probe current. The left part of the spectrum is symmetrical to the right part (the spectrum is recorded twice), the central peak is the frequency marker $f_m = 0$, and the coordinate scales are linear. The conditions are the same as in Fig. 3; a – state I, outermost peaks – frequency markers $f_M = 200$ kcs; b – state II, side peaks – at frequencies 95, 190, 285 kcs; c – state III, outermost peaks – frequency markers $f_M = 4$ Mcs.

probe is zero, and the probe current is due predominantly to the electrons). We see that the oscillation spectrum consists generally speaking of two parts—line and continuous.

The line part of the spectrum includes a set of harmonics of a certain fundamental frequency $f_0$; this frequency changes relatively little (increases) in the transition I → II (usually by not more than a factor 1.5—2), but in the transition II → III it increases by another factor 5—10. In absolute magnitude, the frequency $f_0$ usually amounts to 30—50 kcs in state I, 50—100 kcs in state II, and 300—500 kcs in state III; in the latter case $f_0$ increases with increasing discharge voltage. The relation between the amplitudes of the oscillations at the frequency $f_0$ and its harmonics depends essentially on the radius R of the probe: the greatest content of higher harmonics is observed at radii close to the place of maximal radial gradient of density of the fast electrons; for state III this is shown in Fig. 7. In many cases the line part of the spectrum contains, in addition to frequency $f_0$ and its harmonics, also oscillations with lower frequency—in the range 1—20 kcs. For state I this is shown in Fig. 6a. Under certain conditions and for sufficiently large R (on the order of several centimeters), these oscillations can prevail over all others.

The continuous part of the spectrum is most pronounced in state III, when it usually occupies the frequency range from several times 10 kcs to 3—5 Mcs. We wish to emphasize here the arbitrariness of the term "frequency range." When using this term, we have in mind an oscillogram similar to Figs. 6 and 7 (the ordinate scale is linear), on which the amplitudes of the oscillations at all frequencies do not go beyond the limits of the oscilloscope screen of the analyzer (that is, the sensitivity of the analyzer is far from maximal). With such a definition of the term "frequency range" (in accordance with Fig. 6) we can state that in states I and II there are no higher frequencies ($f \gtrsim 0.5$—1 Mc) in the oscillation spectrum. However, if we take this term to mean the entire frequency range in which the amplitude of the oscillation differs from the measurement errors, then the "frequency range" is appreciably broadened. In fact, if we increase the sensitivity of the analyzer by a factor of several times, then the oscillation spectrum shown in Fig. 7 assumes the form shown in Fig. 8.

At maximum analyzer sensitivity the "frequency range" in all three states of the beam is almost the same—of the order of 20—30 Mc (in state I it

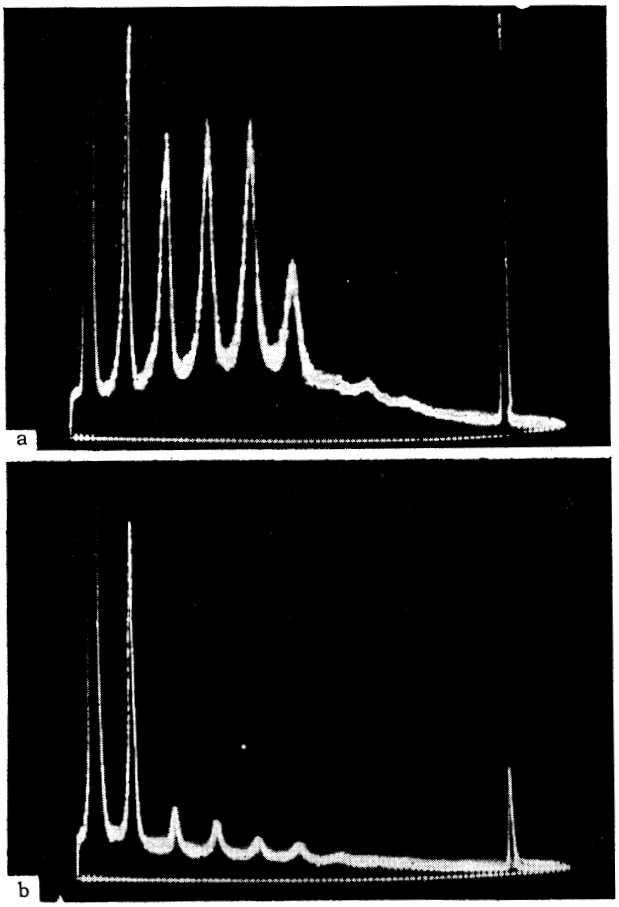


FIG. 7. Spectra of probe current oscillations for two probe radii: a – R = 15 mm, b – R = 2 mm. The outermost peaks are frequency markers $f_M = 0$ and $f_M = 4$ Mc. State III, conditions the same as in Fig. 3, $Q < Q_1$.

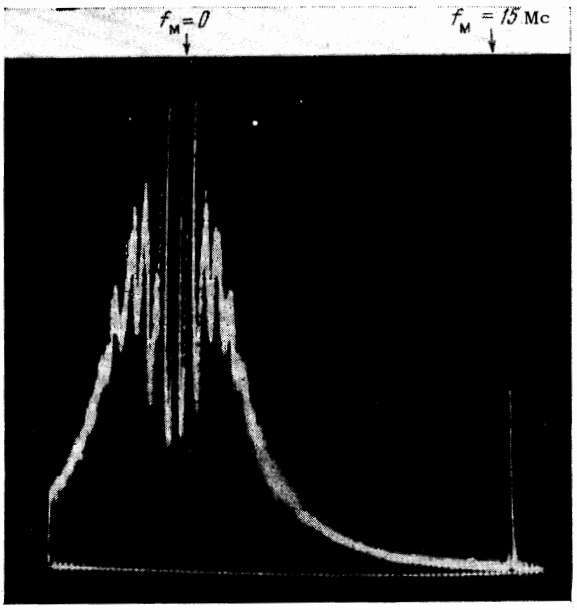


FIG. 8. Spectrum of the oscillation of the probe currents in state III. Conditions are the same as in Fig. 7, but the sensitivity of the analyzer has been increased by a factor of several times. The central and outer right peaks – frequency markers $f_M = 0$ and $f_M = 15$ Mc.

is many times narrower than in state III). However, the "specific gravity" of the high-frequency oscillations in state I is exceedingly small compared with state III. For example, the ratio of the amplitude of the high-frequency (continuous) portion of the spectrum (f = 1—2 Mc) to the amplitude of the oscillations at frequency $f_0$ in state I is several hundred times smaller than in state III; the latter can also be seen from Fig. 6.

The continuous part of the oscillation spectrum obtained with the aid of the annular electrode has the same form as the spectrum of the Langmuir probe, but the line part of the spectrum is less rich in harmonics, for it usually contains principally the frequency $f_0$.

Thus, from the foregoing comparison of the properties of the plasma beam in different discrete states we see that earlier [1-4] when speaking of an unstable plasma beam, we had in mind state III, in which condition (2) is satisfied; state I, which satisfies criterion (1), has been designated as stable. State II, which previously has not been investigated, is intermediate between I and III: on the one hand, the ions become accelerated in this state, as in III; on the other hand, in this state, as in I, there is no virtual cathode. This state precedes directly the transition of the beam into state III.

The experimental data presented above were obtained in experiments with argon. The substitution of hydrogen for argon yielded no new qualitative effect and led only to small quantitative changes: for example, smaller jumps in the quantities $j_e$, $j_+$, $I_a$, and $\alpha$, smaller spreading of the beam and the plasma in the transitions I → II → III, etc. The main reason for using argon in most of the experiments was the fact that the intermediate state II was easier to obtain.

We note that jumplike transitions between the discrete states of the plasma beam exhibit a hysteresis: the numerical values $Q_1$ and $Q_2$ depend on the sign of the change of Q. Thus, when Q increases these quantities are equal to those shown in Fig. 3, and when Q decreases they are 15—20 per cent lower. When hydrogen is substituted for argon, the gas flow necessary to maintain the discharge decreases, naturally, and the values of $Q_1$ and $Q_2$ correspondingly increase.

To study the nature of the beam instability in question, we carried out several experiments which led to the following results:

First, it turned out that the beam could exist in state III only when its length $L_b$ exceeded a certain minimal (or 'critical') value $L_c$, of the order of 25—30 cm. This is seen from Fig. 9, which shows the dependence of the floating potential of the annular electrode $\varphi_r$ on the length of the beam. When $L_b > L_c$ the amplitude of the oscillations of the anode current amounts to several dozen per cent of the discharge current $I_{dis}$; when $L_b < L_c$ and $L_b \gg L_c$ this amplitude is several times smaller.

Second, when $L_b > L_c$ the oscillation spectrum (both the line and the continuous parts) in all three states of the beam does not depend to any appreciable degree on $L_b$, or on the ion mass M (argon, hydrogen). This means that these are not ion-sound oscillations, for otherwise the oscillation frequency would change in proportion to $1/L_b\sqrt{M}$, [5] something not observed in the experiments. The dependence of the oscillation spectrum on the magnetic field is likewise weak, and is not of the type that would cause us to assume the oscillations to be of the ion-cyclotron or of the Alfven type.

Third, the oscillograms of the currents in the probes 1, 2, and 3 are similar; the phases of the oscillations on these probes are the same if the probes are in the same azimuth; when probe 3 is shifted in azimuth, a phase shift is observed in the signal from this probe relative to the signals of probes 1 and 2: for the fundamental frequency this phase shift is equal to the angle of probe rotation, for the second harmonic it is twice as large, etc. The sign of the change in the phase shift with rotation of probe 3 corresponds to rotation of the azimuthal inhomogeneity of the plasma density ("torch") to the "ionic" side. These regularities were observed in all three states of the beam and are valid for any preferred frequency of the line part of the spectrum.

Fourth, it turns out that the transition from the beam-electron velocity distribution $f_1(v)$ in the "direct arc" mode to $f_2(v)$ in the "reflected arc" mode (Fig. 2) causes no essential change in spectrum in each of the three investigated discrete states of the plasma beam. This result is of interest in connection with the question of the

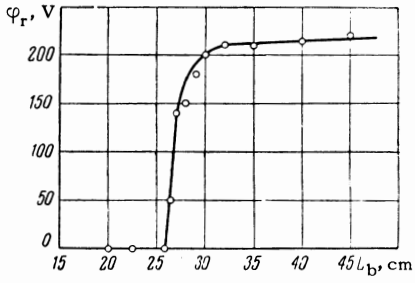


FIG. 9. Dependence of the negative floating potential of the ring electrode $\varphi_r$ on the distance $L_b$ between the source cathode and the anode. The conditions are the same as in Fig. 3, $Q < Q_1$.

degree to which the plasma-beam instability in question is connected (if at all) with the "usual" two-stream instability which results from the presence of "order" in the motion of the electrons in velocity space [6,7]. To obtain a definite answer to this question it is necessary to investigate the high-frequency electronic ("Langmuir") oscillations in all three states of the plasma beam. We are presently carrying out such an investigation.

On the other hand, it is quite probable that an important role in the excitation of the investigated instability is played by effects connected with the spatial inhomogeneity of the plasma [8-10].

In order to compare the obtained results with data by others it is necessary to note that the different states of the plasma beam were observed also in [11], where they were designated "mode I" and "mode II." The first of these modes corresponds to our state I. Inasmuch as no attempt was made in [11] to observe a virtual cathode, it is difficult to state whether mode II is closer to state II or to state III.

In conclusion we wish to stop and estimate the electric fields and the velocity of the radial drift of the electrons of the primary beam in state III. This estimate can be made by starting from the fact that in the transition I → III the "diameter" of the beam in the anode plane increases by 2—3 cm (Fig. 5), and that such a considerable spreading of the beam occurs within the time of flight of the primary electrons ($\sim 3 \times 10^{-7}$ sec). Assuming that the field under consideration does not have time to change greatly within this time of flight, we obtain the azimuthal component of the field averaged over the length of the beam: $E_\varphi \approx 100$—$200$ V/cm (H = 1400 Oe). This value of the field corresponds to the relation

$$E_\varphi \approx W_1 / ea = V_p / a,$$

where a is the "radius" of the beam. The radial flux of the primary electrons under the influence of such a field, from a unit lateral surface of the beam, amounts to

$$j_r = n_1 c \frac{E_\varphi}{H} \approx n_1 c \frac{W_1}{eHa}.$$

Expressing arbitrarily this flux in the form $j_r = D \times \text{grad } n_1 \approx Dn_1/a$, we obtain the "diffusion coefficient" of the primary electrons transversely to the magnetic field

$$D \approx cW_1 / eH. \qquad (3)$$

If we take as the "natural standard" for comparison the well known "Bohm" diffusion coefficient $D_B = cT_e/16eH$ [12], then we obtain from (3)

$$D / D_B \approx 16 W_1 / T_e \gg 1,$$

i.e., $D \gg D_B$, even if we take $T_e$ equal to $W_1$.

Thus, the plasma-beam instability in question is accompanied by very intense fluxes of electrons transverse to the magnetic field, which turn out to be large even compared with the Bohm diffusion. This circumstance is in agreement with the fact (noted above and in [1,4]) that in state III the greater part of the primary beam travels, in final analysis, transversely to the magnetic field.

It is interesting, incidentally, to note that in the case of the estimate of the field $E_\varphi$ considered here, the primary electron beam, in addition to its main function, also performs the diagnostic role which is sometimes assigned to charged-particle beams purposefully introduced into the plasma in order to sound its electric fields.

We are grateful to A. B. Mikhaĭlovskiĭ for stimulating discussions and V. Piffl for participating in part of the measurements.

[1] M. V. Nezlin, JETP **41**, 1015 (1961), Soviet Phys. JETP **14**, 723 (1962).

[2] M. V. Nezlin and A. M. Solntsev, JETP **48**, 1237 (1965), Soviet Phys. JETP **21**, 826 (1965).

[3] M. V. Nezlin and A. M. Solntsev, JETP **45**, 840 (1963), Soviet Phys. JETP **18**, 576 (1964).

[4] M. V. Nezlin, JETP **46**, 36 (1964), Soviet Phys. JETP **19**, 26 (1964).

[5] I. Alexeff and R. V. Neidigh, Phys. Rev. **129**, 516 (1963).

[6] Ya. B. Fainberg, Atomnaya énergiya **11**, 313 (1961).

[7] I. F. Kharchenko, Ya. B. Faĭnberg, R. M. Nikolaev, E. A. Kornilov, E. I. Lutsenko, and N. S. Pedenko, Nuclear Fusion, Suppl. **3**, 1101 (1962).

[8] A. B. Mikhaĭlovskiĭ, JETP **48**, 380 (1965), Soviet Phys. JETP **21**, 250 (1965). A. B. Mikhaĭlovskiĭ and É. A. Pashitskii, DAN SSSR **165**, No. 4 (1965), Soviet Phys. Doklady, in press.

[9] E. A. Lovetskiĭ and A. A. Rukhadze, Nuclear Fusion **5**, (1965). L. S. Bogdankevich and A. A. Rukhadze, ibid.

[10] V. V. Vladimirov, DAN SSSR **162**, 785 (1965), Soviet Phys. Doklady **10**, 519 (1965).

[11] R. V. Neidigh and C. H. Weaver, Proc. 2-nd Intern. Conf. on Peaceful Uses of Atomic Energy, Geneva, (1958), 31, report 2396 p. 315.

[12] D. Bohm, The Characteristics of Electrical Discharges in Magnetic Fields, edited by A. Guthrie and R. K. Wakerling, N. Y. (1949).

Translated by J. G. Adashko
173